



**Fermilab**

TS-SSC 90-085

Fermi National Accelerator Laboratory  
Technical Support Engineering  
P.O. Box 500 - Batavia, Illinois - 60510

November 6, 1990

TO: SSC 40mm File  
FROM: Jim Kerby, TS / Engineering  
SUBJECT: Finite Element Analysis of End Collet Mechanism

An ANSYS model has been constructed to predict the end collet deflections, and coil pole load decreases, for the preload, cooldown, and excitation load cases for the return end collet, using various spacer and skin materials. This note addresses the return end only, lead end model results will be reported elsewhere. For an overview of the design decisions involved, see TS-SSC 90-067, by Jim Strait.

The finite element model uses frictionless gaps between all components, and linear material properties. The mesh is shown in Figure 1, and pertinent material properties in Table 1. Two different thermal contraction coefficients were used for the radial direction of Azimuthal G-10, one resulting in .006 in/in contraction to 4 ° K and one resulting in .010 in/in contraction (measurements suggest the larger contraction rate is more accurate). Gap elements are used between the inner and outer coils, the coils and pole pieces, the pole pieces and the spacer, the spacer and the skin, and the spacer and the line of symmetry at the horizontal and vertical axes (represented by bold lines on figure 1.). Symmetry boundaries were used at the vertical axis of the pole pieces and the skin, and the horizontal axis of the skin (hash marks). The coil preload was applied by displacing the midplane nodes of the inner coil 0.018" vertically, and the outer coil 0.016" (arrows). For the model with an Azimuthal G-10 spacer, and stainless steel skin (the original design), these resulted in coil preloads of 10737 and 7865 psi, respectively (close to the desired 10000 and 8000 psi desired on the inner and outer coils). The displacement was not changed for the different spacer and skin material cases run, so the initial preload of the coils varies depending on the stiffness of the spacer/skin system.

The model is 2-D only, and assumes a 5T central field (5.5T peak) during excitation. The model represents a portion of the end clamp where the coil has exited the main collar/yoke assembly, but has not yet begun the 3-D turn up and over the beam tube. The model does not account for the varying field in the end region, nor the 3 dimensional support of the coil as it turns. The green putty used at the poles to (currently) fix the splice spatially is assumed to not be a structural member. The initial spacer to spacer gap of

0.032" has been included in the treatment of the gap conductors to ground which bound the spacer segment at the vertical and horizontal planes.

Results have been tabulated in Tables 2 through 7. Tables 2 and 3 present the deflections of the outer surface of the skin, and the preload on the inner and outer coils at the pole, for each of the load cases where the Azimuthal G-10 spacer has been replaced by another, with all other parameters remaining unchanged. Deflections of DS0307 and DS0310 (both Azimuthal G-10), DS0311 (Transverse G-10) under preload (warm), and F5 under excitation are included for comparison, although exact agreement between predictions and measurements is neither expected nor found. Results show the vertical deflection under preload to be very similar for all models, although those with spacers of lower elastic modulus (higher compression) deflect less in the vertical plane than those using stiffer spacer materials. The cooldown deflections are a function of two things, the contraction of the skin material, and the preload loss of the coil. For a free standing stainless steel skin of identical nominal dimension, the expected contraction of the outer radius would be 9.38 mils radially. Vertical contractions greater than this reflect a loss of coil preload, while contractions less than this reflect an increase in the coil preload due to the relative contractions of the skin and spacer and coil materials. Finally, the excitation deflections are very similar to the preload case, where the load is resisted by the spacer and skin stiffness, although in a different direction. Table 3 presents the pole preload losses for the same cases, which provide some corroboration of the effects. These numbers were calculated by summing the compressive load between the coil and pole piece, then dividing by the total area to give average stress values. However, it should be noted that for the cases when the average value of preload has dropped below 3000psi, some portion of the coil pole has unloaded, and generally there is no compressive load across the coil in the inner radius region. For the Azimuthal G-10 (.010) case, this means the coil has completely unloaded after cooldown.

Figure 2 plots the data from Table 3, with the exception of the Azimuthal G 10 (.010) case, which would show an initial value equal to the Azimuthal G-10 (.006) case, then drop to zero for both the cooldown and excitation load cases.

Tables 4 and 5 show deflection and preload data for a stycast spacer, with either a stainless steel or aluminum skin, of the same thickness. The aluminum skin is much more compliant, resulting in higher preload losses, but after cooldown the coil preloads are very similar for both cases, as the aluminum forces the spacer to follow the coil shrinkage better than the stainless skin does. Both systems, however, provide only marginal support when excitation loads are included.

Finally, Tables 6 and 7 provide a comparison of the use of SS and aluminum spacers, and SS and aluminum skins. The aluminum skin runs include two thicknesses (0.2625 and 0.5125"), also. The increased aluminum skin thickness produces preloads almost as high as that for the stainless steel

skin, but produces higher preloads after cooldown, when the aluminum skin contracts at the same rate as the coil. Deflections listed are for the outer radius of the skin, which for the thickened aluminum skin has increased to a radius of 3.375". The free standing contraction for the stainless steel skin, aluminum skin and thickened aluminum skin at the outer radius is then 9.38mils, 12.50 mils, and 13.50 mils, respectively. These results agree well with the predictions for the return end of TS-SSC 90-067.

ANSYS 4.4

SEP 20 1990

09:49:07

PLOT NO. 1

POST1 ELEMENTS

TYPE NUM

ZV =1

DIST=1.719

XF =1.563

YF =1.563

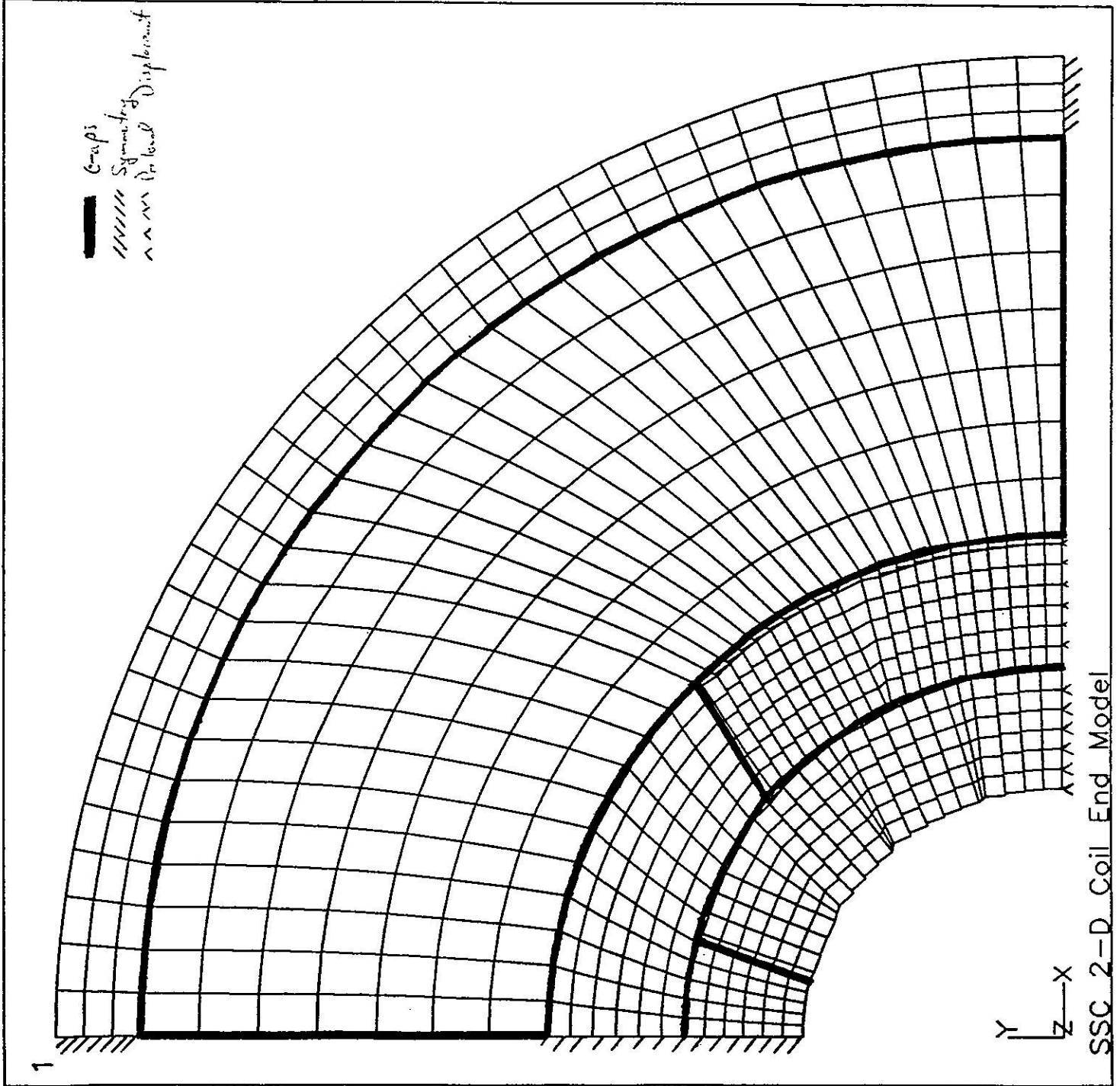


**Table 1. Mechanical Properties**

		<u>E (psi)</u>	<u><math>\alpha</math> (in/in to 4 °K)</u>
Coil/Wedges		1.5e6	.0040
Azimuthal G-10	(Radial)	2.0e6	.0100
	(Radial)	2.0e6	.0060
	(Azimuthal)	4.1e6	.0020
Stycast		1.1e6	.0053
Transverse G-10		4.1e6	.0020
Stainless Steel (316)		28.0e6	.0030
High Mn Stainless Steel		29.0e6	.0017
Aluminum		10.0e6	.0040

**Table 2. Stainless Steel Skin w/ Varying Spacers**  
**(End can deflections)**

<u>Preload</u>	<u>Horiz</u>	<u>Vert</u>		
Azimuthal G-10 Spacer (.010)	-7.62 mils	11.25 mils		
Azimuthal G-10 Spacer (.006)	-7.62	11.25		
Stycast Spacer	-7.96	10.77		
Transverse G-10 Spacer	-7.15	11.77		
Stainless Steel Spacer	-5.96	11.91		
Hi Mn Stainless Steel Spacer	-5.95	11.90		
DS0307 (calipers, @1.5")	-4.	5.		
DS0310 (calipers, @1.5")	-8.75	7.75		
DS0311 (calipers, @1.5")	-6.00	13.75		
<u>Cooldown</u>	<u>Horiz</u>	<u>ΔH</u>	<u>Vert</u>	<u>ΔV</u>
Azimuthal G-10 Spacer (.010)	-17.54	-9.92	-3.52	-14.77
Azimuthal G-10 Spacer (.006)	-17.95	-10.33	-0.72	-11.97
Stycast Spacer	-17.74	-9.78	-0.42	-11.19
Transverse G-10 Spacer	-16.35	-9.20	2.85	-8.92
Stainless Steel Spacer	-15.59	-9.63	2.16	-9.75
Hi Mn Stainless Steel Spacer	-14.66	-8.71	3.33	-8.57
<u>Excitation</u>	<u>Horiz</u>	<u>ΔH</u>	<u>Vert</u>	<u>ΔV</u>
Azimuthal G-10 Spacer (.010)	-2.71	14.83	-18.80	-15.28
Azimuthal G-10 Spacer (.006)	-4.99	12.96	-13.15	-12.43
Stycast Spacer	-3.62	14.12	-13.69	-13.27
Transverse G-10 Spacer	-5.17	11.18	-7.67	-10.52
Stainless Steel Spacer	-5.70	9.89	-7.63	-9.79
Hi Mn Stainless Steel Spacer	-4.88	9.78	-6.29	-9.62
F5 (to 6600A)		5.1		

**Table 4. Stycast Spacer w/ Stainless and Aluminum Skins**  
**(End can deflections)**

<i>Preload</i>	Horiz	Vert		
Stainless Steel Skin	-7.96 mils	10.77 mils		
Aluminum Skin	-5.95	12.98		
<i>Cooldown</i>	Horiz	$\Delta H$	Vert	$\Delta V$
Stainless Steel Skin	-17.74	-9.78	-0.42	-11.19
Aluminum Skin	-19.36	-13.41	-0.12	-13.10
<i>Excitation</i>	Horiz	$\Delta H$	Vert	$\Delta V$
Stainless Steel Skin	-3.62	14.12	-13.69	-13.27
Aluminum Skin	-3.12	16.24	-14.76	-14.64

**Table 5. Stycast Spacer w/ Stainless and Aluminum Skins**  
**(Pole preloads)**

<i>Preload</i>	Inner	Outer		
Stainless Steel Skin	9441 psi	6639 psi		
Aluminum Skin	6910	4307		
<i>Cooldown</i>	Inner	$\Delta I$	Outer	$\Delta O$
Stainless Steel Skin	5196	-4245	4739	-1900
Aluminum Skin	5189	-1721	4660	353
<i>Excitation</i>	Inner	$\Delta I$	Outer	$\Delta O$
Stainless Steel Skin	3034	-2162	4226	-513
Aluminum Skin	2890	-2299	4010	-650

**Table 6. Stainless and Aluminum Spacers and Skin**  
**(End can deflections)**

<u>Preload</u>	<u>Horiz</u>	<u>Vert</u>		
SS spacer / SS skin	-5.96 mils	11.91 mils		
Alum spacer / SS skin	-6.52	11.94		
SS spacer / Alum skin	-4.11	14.38		
Alum spacer / Alum skin	-4.42	14.27		
SS spacer / Alum skin (2x)	-3.63	11.24		
Alum spacer / Alum skin (2x)	-4.03	11.24		
<u>Cooldown</u>	<u>Horiz</u>	<u><math>\Delta H</math></u>	<u>Vert</u>	<u><math>\Delta V</math></u>
SS spacer / SS skin	-15.59	-9.63	2.16	-9.75
Alum spacer / SS skin	-16.67	-10.15	1.33	-10.61
SS spacer / Alum skin	-15.86	-11.75	3.68	-10.70
Alum spacer / Alum skin	-17.17	-12.75	2.41	-11.86
SS spacer / Alum skin (2x)	-16.49	-12.86	-0.94	-12.18
Alum spacer / Alum skin (2x)	-17.74	-13.71	-1.75	-12.99
<u>Excitation</u>	<u>Horiz</u>	<u><math>\Delta H</math></u>	<u>Vert</u>	<u><math>\Delta V</math></u>
SS spacer / SS skin	-5.70	9.89	-7.63	-9.79
Alum spacer / SS skin	-6.05	10.62	-9.01	-10.34
SS spacer / Alum skin	-3.93	11.93	-7.85	-11.53
Alum spacer / Alum skin	-4.51	12.66	-9.59	-12.00
SS spacer / Alum skin (2x)	-7.98	8.51	-9.25	-8.31
Alum spacer / Alum skin (2x)	-8.65	9.09	-10.51	-8.76

**Table 7. Stainless and Aluminum Spacers and Skin**  
(Pole preloads)

<u>Preload</u>	Inner	Outer		
SS spacer / SS skin	12768 psi	9869 psi		
Alum spacer / SS skin	12444	9520		
SS spacer / Alum skin	8302	5683		
Alum spacer / Alum skin	8184	5553		
SS spacer / Alum skin (2x)	10975	8323		
Alum spacer / Alum skin (2x)	10744	8075		
<u>Cooldown</u>	Inner	$\Delta I$	Outer	$\Delta O$
SS spacer / SS skin	10355	-2413	9648	-221
Alum spacer / SS skin	8757	-3687	8118	-1402
SS spacer / Alum skin	8302	0	7658	1975
Alum spacer / Alum skin	7362	-822	6751	1198
SS spacer / Alum skin (2x)	11367	392	10685	2362
Alum spacer / Alum skin (2x)	10006	-738	9368	1293
<u>Excitation</u>	Inner	$\Delta I$	Outer	$\Delta O$
SS spacer / SS skin	7711	-2644	9174	-474
Alum spacer / SS skin	6118	-2639	7676	-442
SS spacer / Alum skin	5495	-2807	7060	-598
Alum spacer / Alum skin	4658	-2704	6149	-602
SS spacer / Alum skin (2x)	8698	-2669	10064	-621
Alum spacer / Alum skin (2x)	7276	-2730	8773	-595

Distribution:

R. Bossert  
D. Delchamps  
W. Koska  
J. Strait  
M. Wake

